attack from adventitious chemical agents.

Collectively, the thermal stability and read-write cycling data indicate that the porphyrin-based information-storage medium is extremely robust. This stability indicates that these constructs can be readily adapted to current semiconductor fabrication technology and operated under the conditions required for a practical device. These characteristics augur well for the use of selected porphyrin molecules in hybrid molecular-semiconductor electronic devices.

References and Notes

1. A. Aviram, M. A. Ratner, *Chem. Phys. Lett.* **29**, 277 (1974).
2. K. S. Kwok, J. C. Ellenbogen, *Mater. Today* **2002**, 28 (2002).
3. R. L. Carroll, C. B. Gorman, *Angew. Chem. Int. Ed.* **41**, 4378 (2002).
4. *International Technology Roadmap for Semiconductors* (Semiconductor Industry Association, San Jose, CA, 2000).
5. The requirement for electronic components to be stable at elevated operating temperatures stems from the facts that (i) heat dissipation in current chips causes operating temperatures to reach as high as 85°C and (ii) these components must function in harsh external environments with extremes in temperature. The latter requirement prevails regardless of whether components can be designed wherein the intrinsic heat dissipated is small during device operation.
6. The fastest dynamic random access memories (DRAMs) can be randomly cycled about once every 20 ns. This time is a "row cycle time" that senses a full row of DRAM cells. A full row can be anywhere from 2000 K to 64,000 K cells, depending on the device. In a computer with 10^9 memory cells, it would take ~300 μs to read the entire memory (provided that 64 K cells could be read in each 20-ns cycle). Therefore, in the 10-year lifetime that is expected of modern memory (*4*), the entire memory could be subjected to as many as 10^{12} cycles. In contrast, if a memory cell could endure only 10^6 cycles, every one of the 10^9 memory cells would fail in the first 10 min of operation.
7. K. M. Roth *et al.*, *J. Vac. Sci. Technol. B* **18**, 2359 (2000).
8. D. Gryko *et al.*, *J. Mater. Chem.* **11**, 1162 (2001).
9. K. M. Roth *et al.*, *Langmuir* **18**, 4030 (2002).
10. K. M. Roth *et al.*, *J. Am. Chem. Soc.* **125**, 505 (2003).
11. A. Balakumar *et al.*, *J. Org. Chem.*, in press.
12. Deep-trench capacitors in DRAM cells typically hold ~40 fF at 1.5 V (*16*). The leakage rates of these capacitors requires that the cell be refreshed at least every 100 ms. As device sizes decrease further, the leakage rates will increase, thereby increasing the required refresh rate. Unless longer charge-retention times can be achieved in semiconductor-based devices, the refresh characteristics of the device will impose limits on the ultimate feature size. These limits may well be encountered before the device is limited by the failure of the bulk properties of semiconductors that are expected when feature sizes reach tens of nanometers (*2*, *3*). In contrast, the charge-retention characteristics of porphyrins are an intrinsic molecular property. Hence, the charge-retention time is independent of the size of the memory cell, even for cell dimensions of tens of nanometers, where each cell would contain an ensemble of many hundreds of electrically noninteracting porphyrins (*9*).
13. C. H. Choi *et al.*, *J. Am. Chem. Soc.* **124**, 8730 (2002).
14. H. J. Callot, R. Ocampo, in *The Porphyrin Handbook*, K. M. Kadish, K. M. Smith, R. Guilard, Eds. (Academic, San Diego, CA, 2000), vol. 1, pp. 349–398.
15. J. Fajer, D. Davis, in *The Porphyrins*, D. Dolphin, Ed. (Academic, New York, 1978), vol. IV, pp. 197–256.
16. J. A. Mandelman *et al.*, *IBM J. Res. Dev.* **46**, 187 (2002).

17. This work was supported by the Defense Advanced Research Projects Agency Moletronics Program (MDA972-01-C-0072) and by ZettaCore, Incorporated. We thank K. Mobley (ZettaCore, Incorporated) for insightful comments on DRAM operating characteristics.

21 August 2003; accepted 9 October 2003

Structure-Based Carbon Nanotube Sorting by Sequence-Dependent DNA Assembly

Ming Zheng,[1]* Anand Jagota,[1] Michael S. Strano,[2] Adelina P. Santos,[3]† Paul Barone,[2] S. Grace Chou,[3] Bruce A. Diner,[1] Mildred S. Dresselhaus,[3] Robert S. Mclean,[1] G. Bibiana Onoa,[1] Georgii G. Samsonidze,[3] Ellen D. Semke,[1] Monica Usrey,[2] Dennis J. Walls[1]

Wrapping of carbon nanotubes (CNTs) by single-stranded DNA (ssDNA) was found to be sequence-dependent. A systematic search of the ssDNA library selected a sequence d(GT)n, n = 10 to 45 that self-assembles into a helical structure around individual nanotubes in such a way that the electrostatics of the DNA-CNT hybrid depends on tube diameter and electronic properties, enabling nanotube separation by anion exchange chromatography. Optical absorption and Raman spectroscopy show that early fractions are enriched in the smaller diameter and metallic tubes, whereas late fractions are enriched in the larger diameter and semiconducting tubes.

CNT separation is an enabling step for many potential applications and fundamental studies that require defined nanotube structures and properties (*1*–*5*). CNTs can be classified into two categories on the basis of their electronic structures: metallic and semiconducting tubes. The latter can be further classified by tube diameters, because the band gap of a semiconducting tube, a critical parameter that needs to be controlled for nanoelectronic applications, is inversely proportional to its diameter. Reports in the literature indicate that it is possible to separate metallic from semiconducting tubes by taking advantage of differences in their physical or chemical properties (*6*–*8*). Diameter-based separation is more difficult, because differences in the physical and/or chemical properties caused by diameter changes are smaller and because variations in tube length could be a dominant factor in physical-based separation methods (*9*–*11*). Here, we report our discovery of an oligonucleotide sequence that self-assembles into a highly ordered structure on CNTs, allowing not only markedly improved metal from semiconducting tube separation but also diameter-dependent separation.

We have previously reported that single-stranded DNA (ssDNA) interacts strongly with CNTs to form a stable DNA-CNT hybrid that effectively disperses CNTs in aqueous solution (*6*). One important issue not addressed previously is whether or not DNA wrapping on a CNT is dependent on the specific sequence of the DNA strand. Here, we found that anion exchange chromatography provides a macroscopic means to assay for electrostatic properties of nanoscale DNA-CNT hybrids. More specifically, we found that the outcome of anion exchange–based DNA-CNT separation, as measured by optical absorption spectral changes from fraction to fraction, is strongly dependent on the DNA sequence. To explore this dependence, we conducted a systematic but limited search of the huge ssDNA library under identical chromatographic conditions. The CNT dispersion procedure is a slight modification of that reported before (*6*). We found that sonication (i.e., disruption with sonic waves) effectively cuts CNTs in the presence of DNA and that short CNTs increase sample recovery from an anion exchange column. In a typical dispersion experiment, a DNA-CNT mixture was kept in an ice-water bath and sonicated (Sonics, VC130 PB, Newton, CT) for 120 min at a power level of 8 W. The average length of CNTs after this level of sonication is ~140 nm, as measured by atomic force micoscopy (AFM). CNTs were "as produced HiPco (high pressure CO)" type from Carbon Nanotechnologies Inc. (Houston, TX), and DNAs were custom-made by Integrated DNA technologies, Inc. (Coralville, IA). We tested simple homopolymers of dA (deoxyadenylate), dC (deoxycytidylate), and dT (deoxythymidylate), as well as sub-libraries composed of totally random combinations of two of the four nucleotides [dG (deoxyguanylate), dA, dT, dC]: poly d(A/C), poly d(A/G), poly d(A/T), poly d(C/T), poly d(C/G), and poly d(G/T). Among these, poly d(G/T) and poly d(G/C) showed the largest variation in the optical absorption spectra from fraction to fraction. To narrow down the choice

[1]DuPont Central Research and Development, Experimental Station, Wilmington, DE 19880, USA. [2]Department of Chemical and Biomolecular Engineering, University of Illinois at Urbana-Champaign, Urbana, IL 61801, USA. [3]Department of Physics, Electrical Engineering and Computer Science, Massachusetts Institute of Technology, Cambridge, MA 02139, USA.

*To whom correspondence should be addressed. E-mail: ming.zheng@usa.dupont.com

†Permanent address: Cento de Desenvolvimento da Tecnologia Nuclear, CDTN/CNEN, Belo Horizonte-MG, 30123-970, Brazil.

of sequence, we then tested representative sequences in the poly d(G/T) and poly d(G/C) sub-library. We found that the best separation was obtained with a sequence of repeats of alternating G and T, d(GT)n, with total length ranging from 20 to 90 bases (n = 10 to 45). Figure 1 shows the elution profile of a d(GT)20-CNT solution from a strong anion exchange column. The first relatively narrow peak corresponds to free DNA, the second broad peak to DNA-CNT hybrids. The resolved features in the broad peak are indicative of an inhomogeneous population of species being fractionated.

Figure 2 shows the ultraviolet-visible–near infrared (UV-Vis-near IR) absorption spectra of fractionated DNA-CNTs. We take the systematic spectral change from early fractions to late fractions as direct evidence for structure-based CNT separation. Three regions are identified in Fig. 2, according to extensive studies reported in the literature for HiPco-type CNTs (*12*–*14*): first interband transitions for metals, M_{11} (400 to 650 nm), and first and second interband transitions for semiconductors, S_{11}(900 to 1600 nm) and S_{22} (550 to 900 nm), respectively. The starting material yielded a spectrum typical of singly dispersed CNTs in aqueous solution, with multiple peaks arising from different types of CNTs overlapping across the entire spectrum. In contrast, the spectrum from an early fraction f35 has only one major peak centered at 980 nm in the S_{11} region, corresponding to the S_{11} transition from the smallest diameter semiconducting tubes found in HiPco CNTs. Additionally M_{11} transitions are enhanced, indicating an enrichment in metallic tubes. The S_{11} region from later fractions (f36, f39, and f45) shows a systematic shift of intensity toward longer wavelength. Because, to a first approximation, the S_{11} transition wavelength is proportional to the tube diameter (*2*), the observed shift indicates a gradual increase in average semiconducting tube diameter from early to late fractions. There is also a simultaneous decrease in the M_{11} intensities in late fractions, corresponding to a depletion of metallic tubes.

The overlapping transitions in the absorption spectra from different types of tubes can be resolved by resonance Raman spectroscopy, providing a means to monitor changes of individual CNT tube types in the separation process. Raman spectroscopy with six excitation wavelengths (457, 501.9, 514.5, 532, 633, and 785 nm) was used to probe the metallic and semiconducting nanotubes in each fraction. We focused on the Raman radial breathing mode, because it is a direct measure of tube diameter, in most cases allowing for the monitoring of a particular (n,m) nanotube during the separation process (*15*). This is aided by recent spectral assignments of metallic (*14*) and semiconducting (*13*) nanotubes. A total of 29 different types of tubes were resolved. Representative spectra are shown in Fig. 3, A and B, which plot the radial breathing mode region with excitation at 785 and 501.9 nm, resonating with a population of semiconducting and metallic nanotubes, respectively. These data show that from early to late fractions, there is a gradual increase in diameter for semiconducting tubes (Fig. 3A) and a gradual depletion of metallic tubes (Fig. 3B).

We developed a quantitative analysis for average tube diameter in each fraction based on Raman data. A nanotube feature of intensity I_{fn} in a fraction fn can be normalized against its intensity I_{f0} in the starting material f0 by the ratio I_{fn}/I_{f0}, which gives the relative tube concentration in fn. The average tube diameter in fn can be defined as a normalized weighted sum over all N nanotubes probed at different Raman wavelengths, as follows

$$< d > = \frac{\sum_{i=1}^{N} \left(\frac{I_{fn}}{I_{f0}}\right) f(d_i) d_i}{\sum_{i=1}^{N} \left(\frac{I_{fn}}{I_{f0}}\right)_i f(d_i)}$$

where $f(d)$ is the diameter distribution in the starting material and is modeled as a normal distribution with a mean diameter of 0.93 nm and a variance of 0.2 nm. This expression gives an average diameter of 0.93 nm for f0, consistent with the model assumption, and gives 0.816 nm, 0.884 nm, 0.958 nm, and 1.084 nm for the semiconducting tubes in f35, f36, f40, and f45, respectively. An evaluation of the metal or semiconductor enrichment was also carried out based on resonance Raman measurements. Such an analysis showed that the content of metallic tubes drops from ~83% in early fractions (f36 and before) to ~10% in late fractions (f43 and after) (figs. S1 to S5).

Diameter-dependent separation allows fundamental studies of energy band structures of CNTs. Our preparative scale separation necessarily deconvolutes the first and second order interband transitions for semiconducting tubes, providing a clear mapping between these features for single nanotube types. By spectral fitting of the absorption spectra (Fig. 2) from the fractionated samples, we estimated that, over the diameter range explored in this work, the ratio of the E22 to E11 oscillator strengths is approximately 0.6.

To better understand the role of the d(GT)n sequence we chose for CNT separation, we used AFM to study its assembly on CNTs. Molecular modeling suggests that ssDNA can adopt many different modes of binding to CNTs, with little difference in binding free energies (*6*). These modes include helical wrapping with different pitches,

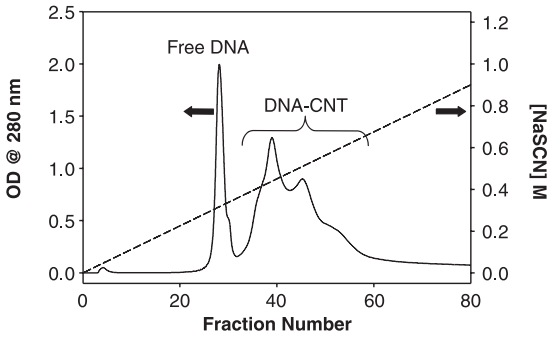

Fig. 1. Chromatogram of anion exchange separation of d(GT)20-CNT. Solid line, optical absorption of the elution at 280 nm; dashed line, the NaSCN concentration gradient. A volume of 800 μl of d(GT)20-dispersed carbon nanotubes at a concentration of ~400 μg/ml was injected into a strong anion exchange column NS1500 (75 mm by 7.6 mm; Biochrom Labs, Inc., Terre Haute, IN), mounted on a BioCAD/SPRINT HPLC system (Applied Biosystems, Foster City, CA), and eluted with a linear salt gradient (0 to 0.9 M NaSCN in 20 mM MES buffer at pH 7) in a 40 ml volume at a flow rate of 2 ml/min. Fractions were collected in 0.5 ml aliquots. When combined, the collected fractions gave an identical absorption spectrum to the starting material, but with a ~70% drop in spectral intensity, indicating irreversible and nonspecific adsorption of DNA-CNT by the column. Arrow associated with each line indicates the corresponding *y* axis.

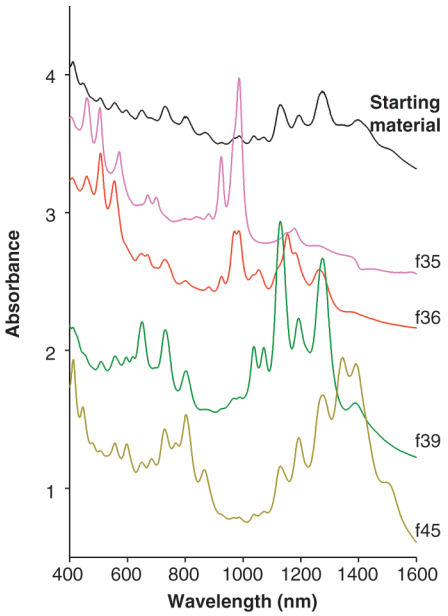

Fig. 2. Absorption spectroscopy on fractionated CNTs. Absorption spectra of the starting material (black), f35 (pink) (4X), f36 (red), f39 (green) (0.5 X), and f45 (olive green) from the experiment described in the text and Fig. 1.

consistent with our observations. In contrast, d(GT)n exhibits a qualitatively different binding to CNTs than most of the other ssDNA sequences. AFM measurements show that d(GT)n-CNT hybrids have a much more uniform periodic structure with a regular pitch of ~18 nm (Fig. 4A; figs. S6 S7). Whatever structure d(GT)n has on CNTs, it appears to be very sensitive to minute changes in the structure of the nucleotide bases. Replacement of G or T by their homologs, inosine or uridine, respectively, decreases the degree of separation on the anion exchange column. Replacing d(GT)n with $d(GGTT)n_{/2}$ that has identical chemical composition also decreases the extent of the separation.

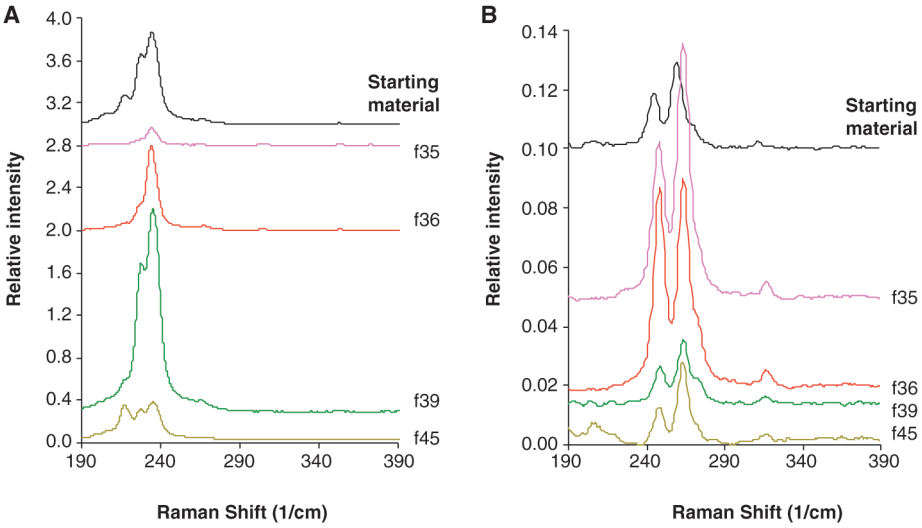

Fig. 3. Raman spectroscopy on fractionated CNTs. Colors are as in Fig. 2. (**A**) Raman spectra obtained using excitation at 785 nm, probing primarily semiconducting tubes. Early fractions show particular enhancement of smaller diameter nanotubes (larger Raman shift at 305 cm^{-1} and 354 cm^{-1}). The opposite is observed for f45 (smaller Raman shift at 218 cm^{-1}). (**B**) Raman spectra obtained using 501.9 nm excitation, probing primarily metallic nanotubes. Fractions f35 and f36 show enhancement of these species.

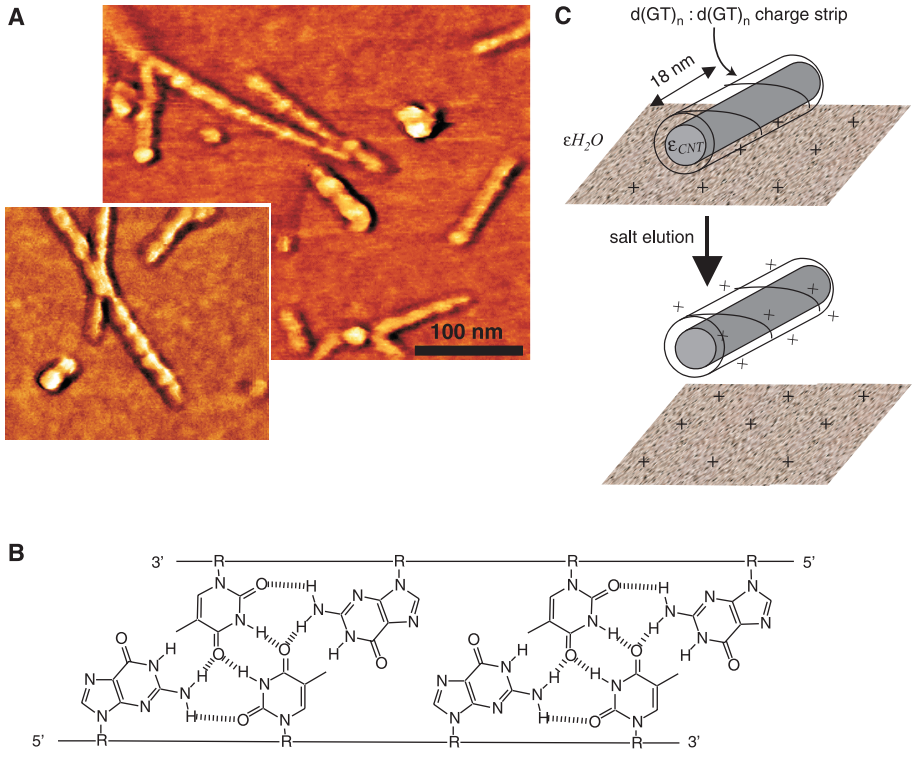

Fig. 4. Mechanism of DNA-CNT separation. (**A**) AFM (phase image) of CNTs wrapped by d(GT)30, showing regular helical pitch of ~18 nm and height of ~2 nm. (**B**) Proposed hydrogen-bonding interactions between two d(GT)n strands that lead to the formation of a "d(GT)n:d(GT)n charge strip." (**C**) Schematic for anion exchange separation process. At lower salt concentration, the surface-bound state is favored in which positive ions on the resin attract the negative surface charge on the DNA-CNT. With increasing salt concentration, the surface and DNA-CNT interactions are screened, favoring elution.

It is known that GT-rich sequences can self-assemble into supramolecular structures that play important roles in telomere replication (*16*), and GT-rich sequences have been observed to form nano-wires involving hydrogen-bonding interactions among different strands (*17*). As a model for the d(GT)n-CNT structure, we propose that two antiparallel d(GT)n strands interact with each other through hydrogen bonds to form a double-stranded strip (Fig. 4B), which then wraps around the CNT with close-packed bases resembling molecular tiles lying on the side wall of the nanotube (Fig. 4C). Such a double-helical structure is built on the unique hydrogen bonding network between two d(GT)n strands and is expected to be more rigid and to have fewer allowed conformations than a single-helical structure. A rigid DNA structure that creates an identical charge distribution within a given type of nanotube is necessary for successful separation. This is probably why most sequences disperse CNTs but do not give good separation.

The mechanism of separation can be explained by examining electrostatics of the DNA-CNT hybrid and its interaction with the positively charged substrate of the anion exchange resin. The DNA-CNT hybrid carries an effective negative charge because of the deprotonated backbone phosphate groups on the DNA (Fig. 4C). The interactions of the hybrid with the positively charged anion exchange resin and the eluting salt solution are electrostatic in nature, and they depend on linear charge density of the hybrid but not the length (*18*, *19*). Indeed, AFM shows that different fractions have similar length distribution (50 to 500 nm). The effective net linear charge density of the hybrid material is determined first by the linear charge density of the phosphate groups along the nanotube axis. This value is modulated by differences in the electronic character of the nanotube core. For metallic tubes, the discrete negative charges on the DNA create along the tube axis an electrostatic field, which induces positive screening image charges (*20*) in the nanotube. As a result, the net linear charge density of the DNA-CNT hybrid is reduced from that of the DNA wrap alone. For semiconducting tubes, the lower polarizability of the nanotube, compared with that of the surrounding water, results in an increased effective lin-

ear charge density of the DNA-CNT hybrid relative to that of the DNA wrap alone, based on an image charge analysis for adjacent dielectrics (*20*). This fundamental difference in behavior provides ample differentiation between the binding strengths of metallic and semiconducting nanotubes to the anion exchange resin. Among semiconducting DNA-CNTs, there are two (nonexclusive) mechanisms that allow linear charge density to depend on tube diameter. First, because the polarizability of semiconducting nanotubes depends on diameter (*21*), the effective linear charge density is diameter-dependent. Second, the linear charge density of the DNA can change with tube diameter due to wrapping geometry changes. Together, these allow diameter-dependent separation of semiconducting tubes.

In summary, we have found that the attachment of ssDNA to a CNT is dependent on the specific DNA sequence and have shown that this can form the basis for a method for CNT diameter and type separation.

References and Notes

1. M. S. Dresselhaus, G. Dresselhaus, P. C. Eklund, *Science of Fullerenes and Carbon Nanotubes* (Academic Press, San Diego, CA, 1996).
2. R. Saito, G. Dresselhaus, M. S. Dresselhaus, *Physical Properties of Carbon Nanotubes* (Imperial College Press, London, 1998).
3. P. Avouris, *Acc. Chem. Res.* **35**, 1026 (2002).
4. S. Niyogi *et al.*, *Acc. Chem. Res.* **35**, 1105 (2002).
5. H. Dai, *Acc. Chem. Res.* **35**, 1035 (2002).
6. M. Zheng *et al.*, *Nature Mater.* **2**, 338 (2003).
7. D. Chattopadhyay, I. Galeska, F. A. Papadimitrakopoulos, *J. Am. Chem. Soc.* **125**, 3370 (2003).
8. R. Krupke, F. Hennrich, H. v. Lohneysen, M. M. Kappes, *Science* **301**, 344 (2003).
9. J. Liu *et al*, *Science* **280**, 1253 (1998).
10. D. Chattopadhyay, S. Lastella, S. Kim, F. Papadimitrakopoulos, *J. Am. Chem. Soc.* **124**, 728 (2002).
11. S. K. Doorn *et al.*, *J. Am. Chem. Soc.* **124**, 3169 (2002).
12. M. J. O'Connell *et al.*, *Science* **297**, 593 (2002).
13. S. M. Bachilo *et al.*, *Science* **298**, 2361 (2002).
14. M. S. Strano *et al.*, *Nano Lett.* **3**, 1091 (2003).
15. J. L. Sauvajol *et al.*, *Carbon* **40**, 1697 (2002).
16. J. R. Williamson, *Annu. Rev. Biophys. Biomol. Struct.* **23**, 703 (1994).
17. T. C. Marsh, J. Vesenka, E. Henderson, *Nucleic Acids Res.* **23**, 696 (1995).
18. G. S. Manning, *Q. Rev. Biophys.* **2**, 179 (1978).
19. G. S. Manning, *Biophys. Chem.* **101-102**, 461 (2002).
20. J. D. Jackson, *Classical Electrodynamics* (John Wiley & Sons, New York, ed. 3, 1999).
21. L. X. Benedict, S. G. Louie, M. L. Cohen, *Phys. Rev. B* **52**, 8541 (1995).

22. This work comes from the Molecular Electronics group at DuPont CR&D. The DuPont group developed DNA-CNT hybrid materials and CNT separation strategy. The UIUC group and the MIT group independently conducted Raman spectroscopy analysis on fractionated CNT samples. A.P.S. acknowledges partial support from the Brazilian agency CNPq. M.S. acknowledges fundings from the National Science Foundation (grant CTS-0330350), the School of Chemical Sciences of the UIUC, and U.S. Department of Energy (award no. DEFG02-91ER45439).

Supporting Online Material

www.sciencemag.org/cgi/content/full/302/5650/1545/DC1
SOM Text
Table S1
Figs. S1 to S7
References

25 September 2003; accepted 20 October 2003

Oceanic Rossby Waves Acting As a "Hay Rake" for Ecosystem Floating By-Products

Yves Dandonneau,[1]* Andres Vega,[2] Hubert Loisel,[3] Yves du Penhoat,[2] Christophe Menkes[1]

Recent satellite observations of Rossby waves and chlorophyll anomalies propagating in subtropical gyres have suggested that wave-induced upwelling could stimulate photosynthesis. Instead, we show that chlorophyll maxima are located in abnormally warm water, in Rossby wave–induced convergences. This excludes inputs of nutrients from deeper water. We argue that the sea color anomalies are not caused by chlorophyll but by floating particles evolved from the ecosystem and accumulated by Rossby waves, acting as "marine hay rakes," in convergence zones. Such processes may be determinant for the distribution of living organisms in oligotrophic areas.

Subtropical anticyclonic gyres occur in about 40% of the world's oceans and have very low nutrient and chlorophyll levels as well as permanently deep pycnoclines and nutriclines. In these oligotrophic areas, respiration balances and sometimes exceeds photosynthesis (*1*). Primary production is mostly supported by the regeneration of nutrients by the microbial loop, whereas export production remains low all year. Export production estimates based on seasonal geochemical budgets, though low, are not entirely accounted for by the mean upwelling of nutrients to the photic layer (*2*, *3*). Thus, it has been suggested that eddy-induced nutrient pumping to the photic layer (*3*) may account for the remainder of export production.

Recently, large-scale propagations of Rossby waves (RWs) from sea level and concurrent ocean color signals have been observed in all subtropical gyres. Nutrient pumping into the photic layer has been proposed as the mechanism by which RWs could increase chlorophyll concentration in these oligotrophic areas (*4*, *5*). Thus, RWs would act like a "rototiller" by lifting nutrients continuously to the photic layer as they propagate (*6*), accounting for some of the missing production in the subtropical gyres. However, the coupling between the dynamics and chlorophyll anomalies has not been elucidated. Using satellite data, we examine here the relations between RWs and chlorophyll concentration in the south Pacific subtropical gyre. We focus on the area 16°S to 22°S, 120°W to 80°W, where RWs have a marked signature.

A typical case is shown for May 2000 (Fig. 1). Filtered fields of sea-level anomalies (SLAs) induced by RWs (*7*) can be interpreted at first order as inverse variations of thermocline depth (*8*). Consequently, more complex mechanisms such as other baroclinic modes (*9*) are neglected. Then, crests and troughs indicate anticyclonic and cyclonic eddies (Fig. 1B). Divergence or convergence of quasi geostrophic surface current has been derived from SLAs (*10*). It corresponds to regions of upwelling or downwelling, respectively (Fig. 1A), spatially shifted from SLA troughs and crests (Fig. 1B). As expected, minima in sea surface temperature anomaly (SSTA) (*11*) correspond to upwelling and maxima, to downwelling (Fig. 1C). Surprisingly, positive chlorophyll anomalies (ChlA) (*12*) are co-located with convergence and positive SSTA (Fig. 1D). This is unexpected, because increased surface phytoplankton concentration is generally related with upwelling of cold and nutrient-rich water. Nutrient inputs in these convergence areas should be less than anywhere else (*13*), and thus only delayed use by phytoplankton of horizontally advected nutrients might explain chlorophyll maxima in these places. However, the time for surface water to drift from upwelling to downwelling patches (typically one month) is longer than needed by the phytoplankton to use such small amounts of nutrients. Hence, lags between nutrient inputs and their utilization cannot explain that positive ChlAs are located in convergences.

[1]IRD, IPSL/Laboratoire d'Océanographie Dynamique et de Climatologie, 75252 Paris 05, France. [2]IRD, Laboratoire d'Etudes en Géophysique et Océanographie Spatiale, Toulouse, France. [3]MREN- Université du Littoral - Côte d'Opale, UMR 8013, Wimereux, France.

*To whom correspondence should be addressed. E-mail: yd@lodyc.jussieu.fr